.

Compensation of native donor doping in ScN: Carrier concentration control and p-type ScN

Bivas Saha, Magnus Garbrecht, Jaime A. Perez-Taborda, Mohammed H. Fawey, Yee Rui Koh, Ali Shakouri, Marisol Martin-Gonzalez, Lars Hultman, and Timothy D. Sands

Citation: Appl. Phys. Lett. **110**, 252104 (2017); doi: 10.1063/1.4989530
View online: http://dx.doi.org/10.1063/1.4989530
View Table of Contents: http://aip.scitation.org/toc/apl/110/25
Published by the American Institute of Physics

AIP | Applied Physics Letters
Save your money for your research.
It's now FREE to publish with us -
no page, color or publication charges apply.
If your article has the potential to shape the future of applied physics, it BELONGS in Applied Physics Letters

APPLIED PHYSICS LETTERS 110, 252104 (2017)

Compensation of native donor doping in ScN: Carrier concentration control and *p*-type ScN

Bivas Saha,[1,a)] Magnus Garbrecht,[2] Jaime A. Perez-Taborda,[3] Mohammed H. Fawey,[4,5] Yee Rui Koh,[6] Ali Shakouri,[6] Marisol Martin-Gonzalez,[3] Lars Hultman,[2] and Timothy D. Sands[7]

[1]*Department of Materials Science and Engineering, University of California, Berkeley, California 94720, USA*
[2]*Thin Film Physics Division, Department of Physics, Chemistry and Biology (IFM), Linköping University, SE-581 83 Linköping, Sweden*
[3]*Instituto de Microelectrónica de Madrid, IMM-CMM-CSIC, C/Isaac Newton 8, Tres Cantos, 28760 Madrid, Spain*
[4]*Karlsruhe Institute of Technology, Institute of Nanotechnology, Hermann-von-Helmholtz-Platz 1, D-76344 Eggenstein-Leopoldshafen, Germany*
[5]*Joint Research Laboratory Nanomaterials (KIT and TUD) at Technische Universität Darmstadt (TUD), Jovanka-Bontschits-Str. 2, D-64287 Darmstadt, Germany*
[6]*School of Electrical and Computer Engineering and Birck Nanotechnology Center, Purdue University, West Lafayette, Indiana 47907, USA*
[7]*Bradley Department of Electrical and Computer Engineering and Department of Materials Science and Engineering, Virginia Tech, Blacksburg, Virginia 24061, USA*

(Received 20 April 2017; accepted 9 June 2017; published online 21 June 2017)

Scandium nitride (ScN) is an emerging indirect bandgap rocksalt semiconductor that has attracted significant attention in recent years for its potential applications in thermoelectric energy conversion devices, as a semiconducting component in epitaxial metal/semiconductor superlattices and as a substrate material for high quality GaN growth. Due to the presence of oxygen impurities and native defects such as nitrogen vacancies, sputter-deposited ScN thin-films are highly degenerate *n*-type semiconductors with carrier concentrations in the (1–6) $\times 10^{20}\,cm^{-3}$ range. In this letter, we show that magnesium nitride (Mg_xN_y) acts as an efficient hole dopant in ScN and reduces the *n*-type carrier concentration, turning ScN into a *p*-type semiconductor at high doping levels. Employing a combination of high-resolution X-ray diffraction, transmission electron microscopy, and room temperature optical and temperature dependent electrical measurements, we demonstrate that *p*-type $Sc_{1-x}Mg_xN$ thin-film alloys (a) are substitutional solid solutions without Mg_xN_y precipitation, phase segregation, or secondary phase formation within the studied compositional region, (b) exhibit a maximum hole-concentration of $2.2 \times 10^{20}\,cm^{-3}$ and a hole mobility of $21\,cm^2/Vs$, (c) do not show any defect states inside the direct gap of ScN, thus retaining their basic electronic structure, and (d) exhibit alloy scattering dominating hole conduction at high temperatures. These results demonstrate Mg_xN_y doped *p*-type ScN and compare well with our previous reports on *p*-type ScN with manganese nitride (Mn_xN_y) doping. *Published by AIP Publishing.* [http://dx.doi.org/10.1063/1.4989530]

Scandium nitride (ScN) is a promising group III(B)-V indirect bandgap rocksalt semiconductor[1–7] with octahedral coordination. ScN thin films have attracted significant interest in recent years for their potential applications in thermoelectricity,[8–10] as a semiconducting component material in epitaxial single crystalline nitride metal/semiconductor superlattices,[11–15] and as an interlayer for the growth of high quality GaN based devices[16] with reduced dislocation densities.[17,18] Like most other transition metal nitrides (TMNs), ScN is structurally and chemically stable, mechanically hard (23 GPa), and corrosion resistant and possesses an extremely high melting temperature in excess of 2600 °C.[19] Due to its rocksalt (cubic) crystal structure, ScN and rocksalt alloys with AlN, GaN, and InN offer interesting bandgap-engineered semiconductor heterostructures that can be integrated with cubic (rocksalt) substrates.[20] Although controversies persisted about the nature of the ScN electronic structure during the 1990s and early 2000s,[19,21] recent experimental results[2,8,22] and theoretical modeling[1,23] have demonstrated conclusively that ScN has an indirect bandgap of 0.9–1.2 eV and a direct gap of 2.2 eV. ScN and its rocksalt solid solution, $Al_xSc_{1-x}N$, have been developed and utilized in recent years to grow the first epitaxial single crystalline metal/semiconductor multilayers and superlattices based on (Hf,Zr)N/ScN[11–15] and TiN/(Al,Sc)N[24,25] material systems, respectively. In the wurtzite crystal system, $Al_xSc_{1-x}N$ is also attractive for its large piezoelectric response.[26,27] In short, ScN is a promising nitride semiconductor for future applications and deserves attention to harness its full potential for practical devices.

Molecular Beam Epitaxy[4,28–30] (MBE), dc-magnetron sputtering,[2,8,31] hybrid vapor phase epitaxy[5,6,32] (HVPE), and other[33,34] methods have been employed over the years to deposit epitaxial ScN thin films on MgO, Al_2O_3 (sapphire), and Si substrates.[35] As-deposited ScN thin-films deposited with most of these growth techniques result in *n*-type semiconductors having large carrier concentrations in the $\sim 10^{19}$ to $10^{21}\,cm^{-3}$ range due to the presence of impurities.[36] The HVPE method[32] so far has proved to be the most effective in achieving a lower carrier concentration in the $\sim 10^{18}\,cm^{-3}$ range although the films had thickness in 10s of μm due to

[a)]Author to whom correspondence should be addressed: bsaha@berkeley.edu

higher growth rates (100 s of nm/min). Sputter-deposited ScN films are also highly degenerate *n*-type semiconductors with carrier concentrations ranging from $1 \times 10^{20}\,\mathrm{cm}^{-3}$ to $6 \times 10^{20}\,\mathrm{cm}^{-3}$ primarily due to oxygen as impurities arising from background water and/or oxygen during deposition.[2,8] Previous Nuclear Reaction Analysis (NRA) along with Rutherford Backscattering Spectrometry (RBS) measurements has demonstrated[8] that as-deposited ScN films incorporate 1.6±1 at. % oxygen as impurities. Although such unintentional electron doping helps in achieving an extremely high thermoelectric power factor[8,9] of (3.3–3.5) × $10^{-3}\,\mathrm{W/mK}^2$ in the 600–850 K temperature range, it is detrimental for the application of ScN in many other device configurations. For example, metal/semiconductor superlattices intended for thermionic transport require ScN layers with very low carrier concentrations. Moreover, electronic and optoelectronic applications based on *pn* junctions require both carrier types and spatial control over doping levels.[37] The authors have previously demonstrated the reduction of the carrier concentration in ScN and *p*-type $Sc_xMn_{1-x}N$ thin-film alloys.[2] However, the concentration of manganese required to turn ScN into a *p*-type semiconductor was relatively large (11% Mn on Sc sites). Moreover, the hole mobility in *p*-type $Sc_{0.89}Mn_{0.11}N$ was extremely small ($2\,\mathrm{cm}^2/\mathrm{Vs}$), and detailed analyses of electronic properties as a function of temperature were missing.

With a motivation to develop ScN based electronic, plasmonic, and thermoelectric energy conversion devices, we demonstrate here that incorporation of Mg_xN_y in ScN reduces its carrier concentration, converting ScN into a *p*-type semiconductor at high doping levels. The temperature dependent electronic and room temperature optical properties of *n*- and *p*-type $Sc_{1-x}Mg_xN$ thin-film alloys are evaluated across the compositional range ($0 < x < 0.04$).

$Sc_{1-x}Mg_xN$ films were deposited on [001] MgO substrates with a reactive DC-magnetron co-sputtering technique inside a load-locked turbo-molecular pumped high-vacuum deposition system with a base pressure of $\sim 10^{-8}$ Torr (PVD Products, Inc.). The growth chamber had the capability to accommodate four targets and was equipped with three DC power supplies. The Sc (99.998% purity on metal basis) and Mg (99.99% on metal basis) targets had dimensions of 2 in. diameter and 0.25 in. thickness. All depositions were performed with an Ar/N_2 mixture of 6 sccm of N_2 and 4 sccm of Ar at a deposition pressure of 5 mTorr. The targets were sputtered in the constant power mode. The substrates were maintained at 750 °C during deposition, as determined using an infrared pyrometer operated in the wavelength range of 0.8–1.1 μm, together with a thermocouple. The films were $\sim$300 nm in thickness as measured with cross-sectional Scanning Electron Microscopy.

Symmetric X-ray diffraction (XRD) spectra show [see Fig. 1(a)] that the pure ScN and $Sc_{1-x}Mg_xN$ thin-film alloys grow with 002 orientations on the [001] MgO substrates. The *c*-axis lattice constant of the pure ScN film was measured to be 4.52 Å, which is consistent with the previous literature reports.[2–5] The XRD spectra also revealed that incorporation of Mg_xN_y in the ScN matrix did not change the lattice parameter of the films significantly, with the *p*-type $Sc_{0.97}Mg_{0.03}N$ exhibiting a *c*-axis lattice parameter of 4.51 Å. The full-width-at-half-maximum (FWHM) of the rocking curve (ω-scan) of pure-ScN was measured to be 0.83°, indicating a nominally single-crystalline thin-film consistent with previous reports,[3] while for *p*-type $Sc_{0.97}Mg_{0.03}N$, the rocking curve was measured to be 0.67°, suggesting a slightly improved crystalline quality. A reciprocal space X-ray map (RSM) [see Fig. 1(b) for pure-ScN, with $Sc_{1-x}Mg_xN$ thin-film alloys showing the same characteristics] clearly demonstrates that the films were relaxed having the film (012) and the substrate (012) peaks separated very clearly. Such strain relaxation is not surprising given the $\sim$7% lattice mismatch between the $Sc_{1-x}Mg_xN$ thin-films and the MgO substrate. $Sc_xMg_{1-x}N$ films are also expected to exhibit flat-topped mounds on the top-surfaces as was shown for pure-ScN in Ref. 38.

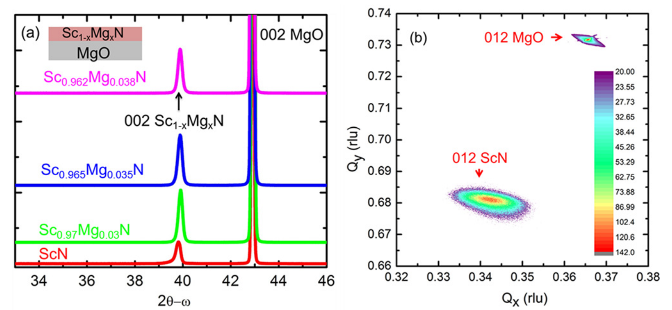

FIG. 1. (a) Symmetric X-ray Diffraction (XRD) spectra of pure-ScN and three p-type $Sc_{1-x}Mg_xN$ thin-film alloys are presented. Like the pure ScN, the p-type alloys grow with 002 orientations on the {001} substrate. No signatures of any secondary phase or impurity clustering were observed in the XRD spectrum. (b) Reciprocal Space X-ray map of a pure ScN film (which is representative of all other n-type and p-type alloys) is presented. The substrate MgO 024 and film 024 peaks are separated along the horizontal axis, which indicates that the films are totally strain relaxed.

High-resolution (scanning)/transmission electron microscopy (HR(S)/TEM) along with Energy Dispersive X-ray spectroscopy (EDS) was employed with the Linköping image- and probe-corrected and monochromated FEI Titan 60–300 microscope equipped with a high-brightness XFEG source and a ChemiSTEM EDS detector system for ultra-high count rates, operating at 300 kV, to characterize the microstructure and composition of the pure-ScN thin film and a representative *p*-type $Sc_{1-x}Mg_xN$ film. A cross-sectional TEM lamella was prepared by a focused ion beam (FIB) using a FEI Strata 400S system equipped with an OmniProbe 200 micromanipulator for in-situ lift-out. Then, the lamella was polished by a focused low-energy argon ion beam using a NanoMill system (model1040, Fischione Instruments). Since the $Sc_{1-x}Mg_xN$ thin films were grown on MgO substrates, traditional composition analysis techniques where the probe beams are directed normal to the surface [such as Rutherford Backscattering Spectrometry (RBS)] are not suitable to separate and determine the composition of Mg in the films from the substrates. HRTEM micrographs of ScN grown on an MgO substrate [presented in Fig. 2(a)] clearly show the well-defined cubic lattices of ScN and MgO, along with a sharp interface. The inset FFT (Fast Fourier Transform) also shows that the ScN films grow on [001] MgO substrates with an epitaxial relationship of (001)[001] ScN||(001)[001] MgO. Images of *p*-type $Sc_{0.97}Mg_{0.03}N$ show very similar characteristics to the pure-ScN, as can be seen in the high-angle annular dark-field (HAADF)-STEM micrograph in Fig. 2(b). Edge dislocations from the lattice

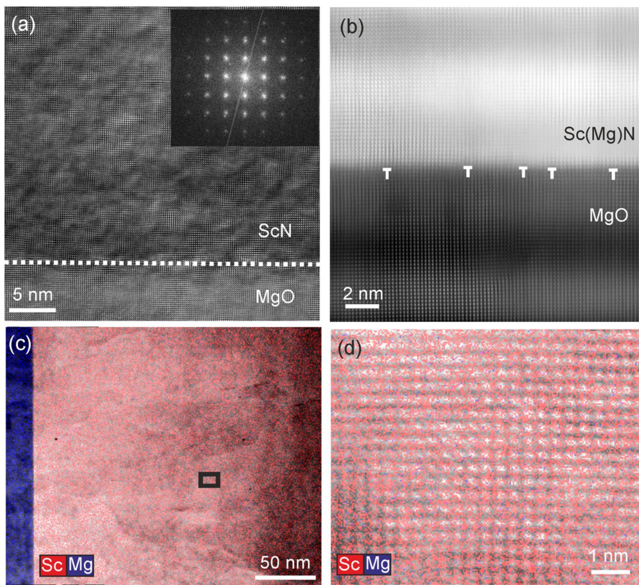

FIG. 2. (a) HRTEM micrograph of an undoped ScN film grown epitaxially on MgO. The quality of growth is demonstrated by the flat and smooth interface, as well by the inset FFT, where the 7% lattice mismatch can be detected by a slight separation of otherwise well-aligned cubic symmetry spots. (b) HAADF-STEM micrograph of a Mg-doped ScN film, showing an atomically flat interface with the MgO substrate, and a few edge dislocations stemming from the lattice mismatch. STEM-based EDS mapping (c) reveals the regular and homogeneous distribution of Mg in the ScN matrix. (d) Atomic resolution EDS map of the area within the rectangular area marked in (c).

mismatch are observed at the interface as expected. STEM-based EDS mapping was performed on both the ScN and $Sc_{0.97}Mg_{0.03}N$ films to determine the spatial distribution of doping (Mg) atoms in the crystal. EDS mapping of the film [Figs. 2(c) and 2(d)] demonstrates uniformly dispersed Mg atoms at low concentrations in the ScN matrix. No signatures of any precipitation or secondary phase formations can be observed. The composition of the films were determined by quantitative EDS analysis employing the *k*-factor method to be between 1.6 and 3.2 atomic % Mg in the ScN matrix (at count rates of ∼450 000 per individual EDS map). The quantitative EDS data were used to benchmark the composition analysis of similar alloy films.

Room temperature electronic and optical properties of pure-ScN and $Sc_{1-x}Mg_xN$ thin-film alloys were measured across the composition range and are presented in Fig. 3. The resistivity of a pure-ScN film was measured to be 0.4 mΩ-cm, which is consistent with previous literature reports.[5,8,9] With the incorporation of Mg_xN_y in the ScN matrix, the resistivity increases by about four-orders of magnitude ($\times 10^4$) before the carrier type changes from the *n*-type (electrons) to the *p*-type (holes). The *n*-type carrier concentrations also decrease with the increase in the Mg concentration inside ScN. Before the films underwent the carrier-type transition, the lowest electron concentration was found to be $\sim 1.3 \times 10^{18}$ cm^{-3}, which is a reduction of ∼25× compared to pure-ScN films. Note that the carrier concentration and mobility of two highly resistive $Sc_{1-x}Mg_xN$ thin-films alloys were not presented. Hall measurements for these two samples (employed for room temperature electronic property analysis in this work) were not useful given the moderate magnetic field (1 Tesla) of our measurement system. These results prove that Mg_xN_y as a substitutional solid solution inside the ScN matrix acts as a hole dopant, reducing the

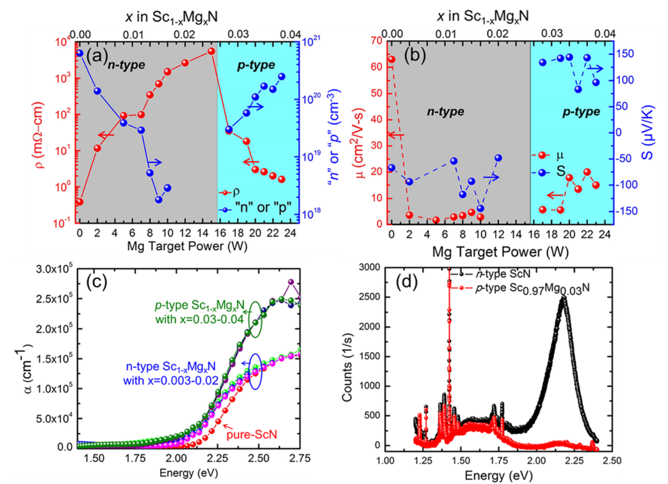

FIG. 3. (a) Electrical resistivity and carrier concentrations as a function of the Mg target power and the concentration of Mg_xN_y in the ScN matrix, measured at room temperature. A clear n-type to p-type carrier transition was observed, accompanied by a decrease in resistivity and changes from electron to hole transport. Note that the carrier concentrations of two highly resistive samples were not listed since the Hall measurement system was ineffective in extracting carrier concentrations for such large resistivity samples due to the limitations in the highest possible magnetic field. (b) Room temperature mobility and Seebeck coefficients of the samples are presented across the composition range. The mobility of the n-type samples decreases clearly due to the incorporation of Mg_xN_y in the ScN matrix but recovers to moderate values for p-type samples. (c) Room temperature optical absorption coefficients for pure ScN and three n-type and three p-type samples are presented. The direct optical bandgap of the alloys remains fixed at 2.21–2.24 eV, while no signatures of any defect states were observed. (d) Photoluminescence (PL) spectra of pure ScN and a p-type $Sc_{0.97}Mg_{0.03}N$ alloy measured at room temperature are presented. The incorporation of Mg_xN_y in the ScN matrix quenches the luminescence of ScN completely.

carrier concentration in the *n*-type films. Based on compositional analysis, the carrier type transition was found to be at ∼2.5%–3% atomic percentage Mg on Sc sites in ScN films. After the carrier transition point, the resistivity of the *p*-type $Sc_{1-x}Mg_xN$ thin films was found to decrease with a further increase in the Mg_xN_y concentrations due to the increasing number of hole carriers, as expected. The lowest observed resistivity in the *p*-type $Sc_{1-x}Mg_xN$ thin films was about 2 mΩ-cm, and the highest hole concentration achieved was 2×10^{20} cm^{-3}. Incorporation of Mg_xN_y in ScN, however, reduced the carrier mobility. Figure 3(b) shows that pure ScN has an electron-mobility of 63 cm^2/Vs; however, with the incorporation of a small amount of Mg_xN_y, the mobility is reduced to below 5 cm^2/Vs. However, the mobility values increase slightly for the *p*-type films. The highest hole-mobility obtained for a *p*-type sample was 21 cm^2/Vs. The room temperature Seebeck coefficient measured across the composition range shows that the pure ScN has a rather moderate but consistent[8,9] Seebeck coefficient of $-73\,\mu$V/K. Within the *n*-type alloy samples, the Seebeck coefficient fluctuates between $-50\,\mu$V/K and $-150\,\mu$V/K; however, the *p*-type samples exhibit higher Seebeck coefficients, at $\sim 140\,\mu$V/K. It is surprising that the Seebeck coefficient does not show a trend with the doping level, while electrical resistivity changes by 4 orders of magnitude for *n*-type samples and one order of magnitude for *p*-type samples. Further work on temperature-dependent Seebeck measurement and multi-band Boltzmann transport will be needed to understand thermoelectric transport in this material.

Room temperature optical properties such as optical absorption and photoluminescence (PL) of pure ScN and the $Sc_{1-x}Mg_xN$ thin-film alloys were also measured. The absorption spectra in the UV-Visible to near-IR spectral range [presented in Fig. 3(b)] show above-direct-bandgap optical absorptions in pure-ScN and in all *n*- and *p*-type $Sc_{1-x}Mg_xN$ thin-film alloys. No signature of any sub-bandgap absorption was observed, which highlights the fact that Mg_xN_y incorporation inside the ScN matrix does not add any defect states inside ScN's direct bandgap or alter its basic band structure. The role of Mg doping was that of an electron acceptor that reduces the carrier concentrations of pure-ScN and eventually leads to *p*-type $Sc_{1-x}Mg_xN$ thin-film alloys. Pure ScN exhibits a direct bandgap of 2.21 eV, which is consistent with our previous report[2] and with reports from other groups.[5,22,39] The $Sc_{1-x}Mg_xN$ thin-film alloys also exhibit a direct gap between 2.21 and 2.24 eV, which clearly supports the hypothesis that the underlying electronic structure is unchanged. One key observation is that the *p*-type $Sc_{1-x}Mg_xN$ alloys exhibit much higher absorption coefficients in comparison to the *n*-type $Sc_{1-x}Mg_xN$ films. The PL spectra of ScN show an emission peak at 2.1 eV corresponding to its direct bandgap with a FWHM of about 0.16 eV. Direct bandgap photoemission from ScN is not expected because of its indirect bandgap nature; however, the observed emission is consistent with our previous observations.[2] Although a detailed explanation of the possible causes of such emission was highlighted in Ref. 2, we mention here that in as-sputtered ScN thin-films, the Fermi energy resides ~0.1 eV above the conduction band-edge (at X valley), which might result in lower thermalization rates for some electrons from the Γ valley to the X valley of the band-structure, compared to the radiative recombination from $\Gamma c - \Gamma v$, thus demonstrating the luminescence. It was observed that the incorporation of Mg_xN_y in ScN decreases the PL intensity dramatically and leads to practically no emission for the *p*-type $Sc_{1-x}Mg_xN$ alloy films. The incorporation of Mg_xN_y is known to lower the Fermi level from the conduction band to inside the bandgap, which would result in faster thermalization and vanishing emission. Some sharp features related to Raman modes and impurities in the MgO substrate were also observed in both the *n*-type and *p*-type samples alike.

The temperature dependent electrical properties of pure-ScN, two *n*-type and three *p*-type $Sc_{1-x}Mg_xN$ alloy films were also measured in the 300 K–850 K range (presented in Fig. 4). However, for the sake of clarity, the temperature dependent electrical properties of pure-ScN and *p*-type $Sc_{0.962}Mg_{0.038}N$ alloy films having the lowest electrical resistivity and the highest hole concentrations are presented in Fig. 4. The resistivity of pure ScN increases by ~3× with the increase in temperature from 300 K to 800 K, suggesting metallic-like conduction characteristics. In a previous publication,[8] the origin of a such increase in resistivity with temperature in pure-ScN has been explained. It was found that the Fermi level of pure-ScN lies above the conduction band-edge by 0.06–0.09 eV due to heavy electron doping from oxygen impurities (and also possibly from nitrogen vacancies). Further modeling analysis employing the Boltzmann transport theory has shown that the temperature dependence of the resistivity could be explained by an acoustic phonon scattering mechanism with a mean free path of ~24 nm at room temperature.

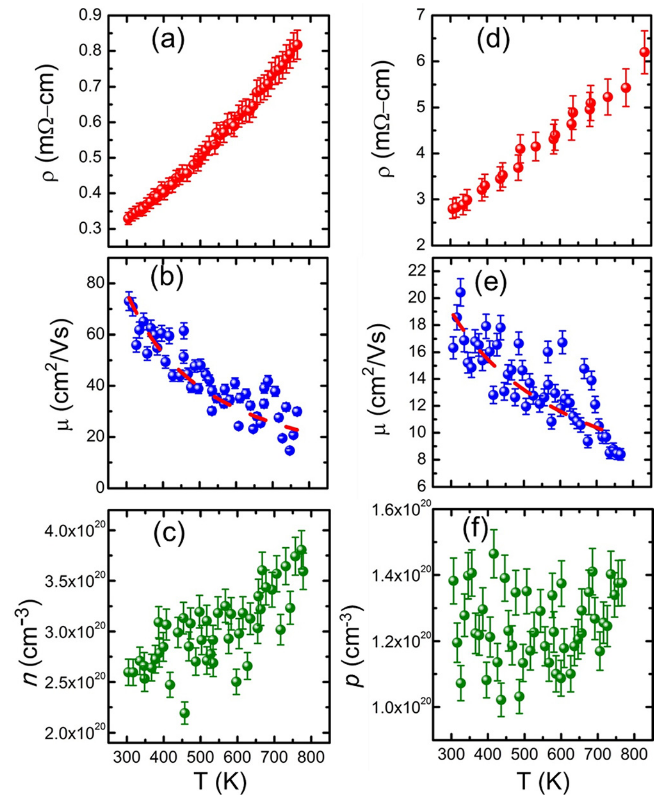

FIG. 4. Temperature dependent electrical resistivity, mobility, and carrier concentration of n-type pure-ScN (a)–(c) and p-type $Sc_{0.962}Mg_{0.038}N$ alloy films (d)–(f) are presented. The resistivity of both the n- and p-type samples increases with temperature due to the presence of the Fermi energy inside the conduction and valence bands, respectively. The electron and hole mobilities decrease with increasing temperature due to the dominant acoustic phonon and alloy scattering, respectively. The carrier concentrations remained relatively unaffected with the increase in temperature.

Apart from our previous report,[8] the metallic like conduction in ScN was reported by Kerdsongpanya *et al.*,[9] where an increase in temperature from 300 K to 800 K increased the resistivity by ~2×. The temperature dependent electrical resistivity in the *p*-type $Sc_{0.962}Mg_{0.038}N$ alloy film also shows an increase as a function of temperature in the 300 K–850 K temperature range. The resistivity of the *p*-type alloy film is about a factor of ten larger than that of pure ScN at room temperature and increased also by a factor of about two over the same temperature range. While detailed modeling analysis on the electrical transport properties of *p*-type $Sc_{1-x}Mg_xN$ and its thermoelectric properties are topics of a future publication,[40] the increase in resistivity as a function of temperature in the *p*-type $Sc_{1-x}Mg_xN$ alloy film suggests that the Fermi energy in the *p*-type $Sc_{0.962}Mg_{0.038}N$ alloy films is expected to be inside the valence band, which gives rise to metallic-like conduction characteristics with holes as dominant carriers.

The temperature dependence of electron and hole mobilities in *n*-type pure ScN and *p*-type $Sc_{0.962}Mg_{0.038}N$ alloy films was also measured, respectively, which would explain their dominant scattering mechanisms in the measured temperature ranges. The mobility decreased from a room temperature (300 K) value of 73 cm^2/Vs to ~20 cm^2/Vs at ~800 K for the pure ScN film, thus exhibiting an ~3.5× decrease, while within the same temperature range, the mobility of the *p*-type $Sc_{0.962}Mg_{0.038}N$ alloy film decreased from ~20 cm^2/Vs to ~8 cm^2/Vs, corresponding to a factor of an ~2.5× decrease.

Fitting the temperature dependent mobility data with $\mu_T = \mu_C T^{\alpha}$ yields an α value of -1.29 for the *n*-type pure ScN and -0.71 for the *p*-type $Sc_{0.962}Mg_{0.038}N$ alloy film. For the pure ScN, $\alpha = -1.29$ suggests the dominance of acoustic phonon scattering on the electron transport at such temperatures and agrees well with the previous[2] modeling assumptions. The exponent α for pure ScN was smaller than that observed for *n*-type semiconductors such as Si and Ge but higher than that of GaAs.[37] Since an ideal semiconductor with acoustic phonon scattering should have exhibited $\alpha = -1.50$, the slightly lower values obtained here indicate possible contributions from optical phonon scattering. The value $\alpha = -0.71$ for the hole mobility of the *p*-type $Sc_{1-x}Mg_xN$ alloy film is consistent with alloy scattering of holes at high temperatures. We note here that the mobility of pure ScN can be enhanced by altering the deposition conditions as was shown in our previous work,[8] which also suggests that the peak mobility values of *p*-type $Sc_{1-x}Mg_xN$ alloy films could be higher. Migration to other deposition techniques such as HVPE may also result in orders of magnitude higher mobility as was shown for *n*-type pure ScN in Ref. 32.

The carrier concentrations of the *n*-type pure ScN and *p*-type $Sc_{0.962}Mg_{0.038}N$ alloy films remain relatively unchanged with the increase in temperature as shown in Figs. 4(c) and 4(f). Such a constant carrier concentration is presumably due to the Fermi level of both the materials residing inside the conduction and valence bands, respectively.

In conclusion, *p*-type $Sc_{1-x}Mg_xN$ substitutional solid-solution alloys have been developed by the incorporation of Mg_xN_y in the ScN matrix. The Mg_xN_y incorporation inside ScN was found to compensate high *n*-type carrier concentrations due to impurities and native defects in ScN and does not introduce defect states inside the bandgap. The development of *p*-type $Sc_{1-x}Mg_xN$ alloys will augment the potential application space for ScN and enable interesting electronic, thermoelectric, and optoelectronic device configurations.

B.S. and T.D.S. acknowledge financial support by the National Science Foundation and U.S. Department of Energy (Grant No. CBET-1048616). M.G. and B.S. acknowledge support from The Swedish Foundation for International Cooperation in Research and Higher Education (STINT). The Knut and Alice Wallenberg (KAW) Foundation is acknowledged for the Electron Microscope Laboratory in Linköping. M.G. and L.H. acknowledge financial support from the Swedish Research Council [RÅC Frame Program (2011–6505), Project Grant No. 2013–4018, and Linnaeus Grant (LiLi-NFM)], as well as the Swedish Government Strategic Research Area in Materials Science on Functional Materials at Linköping University (Faculty Grant No. SFO-Mat-LiU 2009–00971). M.G. acknowledges support in specialized TEM sample preparation at the Karlsruhe Nano Micro Facility (Project ID: 2015–015-010151) by V. S. K. Chakravadhanula. M.M.G. acknowledges financial support by ERC Starting Grant No. NanoTEC 240497 and the INFANTE Project No. 201550E072. J.A.P.T. acknowledges the FPI from the Project PHOMENTA (MAT2011–27911).

[1]B. Saha, J. Acharya, T. D. Sands, and U. V. Waghmare, J. Appl. Phys. **107**, 033715 (2010).
[2]B. Saha, G. Naik, V. Drachev, A. Boltasseva, E. E. Marinero, and T. D. Sands, J. Appl. Phys **114**, 063519 (2013).
[3]D. Gall, I. Petrov, N. Hellgren, L. Hultman, J. E. Sundgren, and J. E. Green, J. Appl. Phys. **84**, 6034 (1998).
[4]H. A. Al-Brithen, A. Smith, and D. Gall, Phys. Rev. B **70**, 045303 (2004).
[5]J. P. Dismukes, W. M. Yim, and V. S. Ban, J. Cryst. Growth **13/14**, 365 (1972).
[6]G. Harbeke, E. Meier, and J. P. Dismukes, Opt. Commun. **4**(5), 335 (1972).
[7]M. A. Moram, Z. H. Barber, C. J. Humphreys, T. B. Joyce, and P. R. Chalker, J. Appl. Phys. **100**, 023514 (2006).
[8]P. V. Burmistrova, J. Maassen, T. Favaloro, B. Saha, S. Salamat, Y. R. Koh, M. S. Lundstrom, A. Shakouri, and T. D. Sands, J. Appl. Phys. **113**, 153704 (2013).
[9]S. Kerdsongpanya, N. van Nong, N. Pryds, A. Zukauskaite, J. Jensen, J. Birch, J. Lu, L. Hultman, G. Wingqvist, and P. Eklund, Appl. Phys. Lett. **99**, 232113 (2011).
[10]S. Kerdsongpanya, B. Alling, and P. Eklund, Phys. Rev. B. **86**, 195140 (2012).
[11]B. Saha, T. D. Sands, and U. V. Waghmare, J. Appl. Phys. **109**, 073720 (2011).
[12]B. Saha, T. D. Sands, and U. V. Waghmare, J. Phys.: Condens. Matter **24**, 415303 (2012).
[13]M. Garbrecht, J. L. Schroeder, L. Hultman, J. Birch, B. Saha, and T. D. Sands, J. Mater. Sci. **51**, 8250 (2016).
[14]M. Garbrecht, B. Saha, J. L. Schroeder, L. Hultman, and T. D. Sands, Sci. Rep. **7**, 46092 (2017).
[15]V. Rawat, Y. Koh, D. Cahill, and T. Sands, J. Appl. Phys. **105**, 024909 (2009).
[16]M. A. Moram, Y. Zhang, M. J. Kappers, Z. H. Barber, and C. J. Humphreys, Appl. Phys. Lett. **91**, 152101 (2007).
[17]M. A. Moram, M. J. Kappers, and C. J. Humphreys, Phys. Status Solidi C **7**, 1778 (2010).
[18]M. A. Moram, C. F. Johnston, M. J. Kappers, and C. J. Humphreys, J. Cryst. Growth **311**, 3239 (2009).
[19]C. Stampfl, W. Mannstadt, R. Asahi, and A. J. Freeman, Phys. Rev. B **63**, 155106 (2001).
[20]B. Saha, S. Saber, G. V. Naik, A. Boltasseva, E. Stach, E. P. Kvam, and T. D. Sands, Phys. Status Solidi B **252**, 251 (2015).
[21]W. R. L. Lambrecht, Phys. Rev. B **62**, 13538 (2000).
[22]R. P. Deng, B. Ozsdolay, P. Y. Zheng, S. V. Khare, and D. Gall, Phys. Rev. B. **90**, 045104 (2015).
[23]A. Qteish, P. Rinke, M. Scheffler, and J. Neugebauer, Phys. Rev. B **74**, 245208 (2006).
[24]B. Saha, G. V. Naik, S. Saber, E. Stach, V. M. Shalaev, A. Boltasseva, and T. D. Sands, Phys. Rev. B **90**, 125420 (2014).
[25]B. Saha, Y. R. Koh, J. Comparan, S. Sadasivam, J. L. Schroeder, M. Garbrecht, A. Mohammed, J. Birch, T. S. Fisher, A. Shakouri, and T. D. Sands, Phys. Rev. B **93**, 045311 (2016).
[26]F. Tasnádi, B. Alling, C. Höglund, G. Wingqvist, J. Birch, L. Hultman, and I. A. Abrikosov, Phys. Rev. Lett. **104**, 137601 (2010).
[27]S. Barth, H. Bartzsch, D. Gloess, P. Frach, T. Herzog, S. Walter, and H. Heuer, IEEE Trans. Ultrason., Ferroelectr., Freq. Control **61**(8), 1329 (2014).
[28]H. Al-Brithen and A. R. Smith, Appl. Phys. Lett. **77**, 2485 (2000).
[29]S. W. King, R. F. Davis, and R. J. Nemanich, J. Vac. Sci. Technol., A: Vac. Surf. Films **32**, 061504 (2014).
[30]T. Ohgaki, K. Watanabe, Y. Adachi, I. Sakaguchi, S. Hishita, N. Ohashi, and H. Haneda, J. Appl. Phys. **114**, 093704 (2013).
[31]D. Gall, I. Petrov, L. D. Madsen, J. E. Sundgren, and J. Green, J. Vac. Sci. Technol., A **16**, 2411 (1998).
[32]Y. Oshima, E. G. Villora, and K. Shimamura, J. Appl. Phys. **115**, 153508 (2014).
[33]W. Lengauer, J. Solid State Chem. **76**, 412 (1988).
[34]Z. Gu, J. H. Edgar, J. Pomeroy, M. Kuball, and D. W. Coffey, J. Mater. Sci.: Mater. Electron. **15**, 555 (2004).
[35]M. A. Moram, S. V. Nokinov, A. J. Kent, C. Norenberg, C. T. Foxon, and C. J. Humphreys, J. Crystal Growth **310**, 2746 (2008).
[36]M. A. Moram, Z. H. Barber, and C. J. Humphreys, Thin Solid Films **516**, 8569 (2008).
[37]S. Adachi, *Properties of Semiconductor Alloys: Group-IV, III–V and II–VI, Semiconductors* (John Wiley & Sons, Chichester, 2009).
[38]P. Burmistrova, D. N. Zakharov, T. Favaloro, A. Mohammed, E. Stach, A. Shakouri, and T. D. Sands, J. Mater. Res. **30**, 626 (2015).
[39]X. Bai and M. E. Kordesch, Appl. Surf. Sci. **175–176**, 499–504 (2001).
[40]B. Saha, J. Anders, Y. R. Koh, J. Bahk, M. M. Gonzalez, A. Shakouri, and T. D. Sands, "Large thermoelectric power-factor in epitaxial n- and p-type scandium nitride (ScN)" (submitted).